

# High-Yield Production of Monolayer FePS<sub>3</sub> Quantum Sheets via Chemical Exfoliation for Efficient Photocatalytic Hydrogen Evolution

Zhongzhou Cheng, Tofik Ahmed Shifa, Fengmei Wang, Yi Gao, Peng He, Kai Zhang,\*  
Chao Jiang, Quanlin Liu, and Jun He\*

2D layered transition metal phosphorus trichalcogenides (MPX<sub>3</sub>) possess higher in-plane stiffness and lower cleavage energies than graphite. This allows them to be exfoliated down to the atomic thickness. However, a rational exfoliation route has to be sought to achieve surface-active and uniform individual layers. Herein, monolayered FePS<sub>3</sub> quantum sheets (Qs) are systematically obtained, whose diameters range from 4–8 nm, through exfoliation of the bulk in hydrazine solution. These Qs exhibit a widened bandgap of 2.18 eV as compared to the bulk (1.60 eV) FePS<sub>3</sub>. Benefitting from the monolayer feature, FePS<sub>3</sub> Qs demonstrate a substantially accelerated photocatalytic H<sub>2</sub> generation rate, which is up to three times higher than the bulk counterpart. This study presents a facile way, for the first time, of producing uniform monolayer FePS<sub>3</sub> Qs and opens up new avenues for designing other low-dimensional materials based on MPX<sub>3</sub>.

monolayer and found a remarkably high value of 625.9 cm<sup>2</sup> V<sup>-1</sup> s<sup>-1</sup> at room temperature,<sup>[9]</sup> which is even higher than other typical 2D materials such as monolayer MoS<sub>2</sub> (200 cm<sup>2</sup> V<sup>-1</sup> s<sup>-1</sup>)<sup>[10]</sup> and WS<sub>2</sub> (214 cm<sup>2</sup> V<sup>-1</sup> s<sup>-1</sup>). Although it is still under development, catalytic applications of nanostructured materials in this family have notable promising features. Theoretical speculations<sup>[9]</sup> reveal that the positions of their conduction and valence bands energy levels straddle the water redox potentials, making them appealing for photocatalyzing water splitting reactions. Moreover, the calculated high carrier mobilities of the 2D MPX<sub>3</sub> materials such as MnPSe<sub>3</sub> indicate that the transfer of carriers to reactive sites would be easier

Owing to their interesting and useful properties, 2D materials, such as graphene,<sup>[1]</sup> MoS<sub>2</sub>,<sup>[2]</sup> and g-C<sub>3</sub>N<sub>4</sub>,<sup>[3]</sup> have led to the increasing attention of scientific communities during the last decades. The size effects exhibited by few-layered nanosheets of these materials result in fundamentally unique properties that substantially differ from their bulk counterparts.<sup>[4]</sup> Nowadays, a new class of 2D layered metal phosphorus trichalcogenides (MPX<sub>3</sub>, where M = Fe, Mn, Ni, etc. and X = S or Se) have received tremendous attentions.<sup>[5–7]</sup> It is gratifying that various important findings have been reported regarding the MPX<sub>3</sub> materials in different applications.<sup>[8]</sup> For instance, Zhang et al., have recently calculated the carrier mobility of 2D MnPSe<sub>3</sub>


in the photocatalytic process, reducing the possibility of electron–hole recombination. It is also important to note that the different kinds of elements in MPX<sub>3</sub> (particularly the chalcogen and the metal atom) give rise to the variation of the bandgaps from 1.3 to 3.5 eV.<sup>[5]</sup> This rich and appropriate bandgaps bring the possibility to efficiently use visible light and design best performing photocatalysts. Our group has recently reported a systematic way of synthesizing ultrathin 2D NiPS<sub>3</sub><sup>[11]</sup> and MnPX<sub>3</sub> (X = S and Se)<sup>[12]</sup> nanosheets. These experimental realizations communicated the promising hydrogen evolving activities of MPX<sub>3</sub> under illumination of simulated solar light without cocatalyst or sacrificial agents. In line with this, the

Z. Z. Cheng, T. A. Shifa, Dr. F. M. Wang, P. He, Prof. C. Jiang, Prof. J. He  
CAS Center for Excellence in Nanoscience  
CAS Key Laboratory of Nanosystem and Hierarchical Fabrication  
National Center for Nanoscience and Technology  
Beijing 100190, China  
E-mail: hej@nanoctr.cn

Z. Z. Cheng, Prof. Q. L. Liu  
School of Materials Science and Engineering  
University of Science and Technology  
Beijing 100083, China  
T. A. Shifa, Prof. J. He  
University of Chinese Academy of Sciences  
Beijing 100049, China

Y. Gao, Prof. K. Zhang  
i-Lab  
Suzhou Institute of Nano-Tech and Nano-Bionics  
Chinese Academy of Sciences  
Suzhou 215123, Jiangsu, P. R. China  
E-mail: kzhang2015@sinano.ac.cn

Y. Gao  
Hubei Collaborative Innovation Center for Advanced Organic Chemical  
Materials–Hubei Key Laboratory of Ferro and Piezoelectric Materials  
and Devices  
Faculty of Physics and Electronic Sciences  
Hubei University  
Wuhan 430062, Hubei, P. R. China

 The ORCID identification number(s) for the author(s) of this article can be found under <https://doi.org/10.1002/adma.201707433>.

DOI: 10.1002/adma.201707433

issue of performance enhancement in photocatalysis is associated with strong light harvesting capability in the visible and near-infrared region, multiple charge carrier generation, and large surface area to volume ratio. Quantum sheets (Qs) are the best candidates to virtually meet these requirements.<sup>[13,14]</sup> Recent studies show that the Qs demonstrate a particularly prominent multiple-exciton generation effect, which is considered as a promising way to reduce heat-related energy losses in solar system by splitting one high-energy photon into multiple low-energy excitons thereby increasing energy conversion efficiency.<sup>[15,16]</sup> Given the very promising features of MPX<sub>3</sub> in catalysis and the attributes of Qs in photochemistry, the design of quantum confined materials in this family is of a great benefit to realize multiply advantageous photocatalyst.

Here, we made use of an important concept to enable us design Qs. That is, most of the MPX<sub>3</sub> compounds have higher in-plane stiffness (60–120 N m<sup>-1</sup>) and lower cleavage energies (0.29–0.54 J m<sup>-2</sup>)<sup>[9]</sup> as compared to graphite (0.37 J m<sup>-2</sup>).<sup>[17]</sup> This suggests that the surface-active MPX<sub>3</sub> nanosheet can be practically exfoliated from the bulk.<sup>[18,19]</sup> Following this, we employ a facile way to exfoliate layered FePS<sub>3</sub> into monolayer Qs with a uniform lateral size of 4–8 nm. Benefitting from our facile exfoliation, the in-plane surface is greatly altered toward exposing more active sites, which is prominent feature of efficient catalysis. Accordingly, photocatalytic test shows that the hydrogen generation rate of the FePS<sub>3</sub> Qs is up to three times (290 μmol g<sup>-1</sup> h<sup>-1</sup>) higher than that of bulk FePS<sub>3</sub> (94 μmol g<sup>-1</sup> h<sup>-1</sup>) under the same illumination conditions.

We believe that, this work opens up a clear avenue for investigation of other members in this family at the level of Qs.

The bulk FePS<sub>3</sub> crystal was synthesized by chemical vapor transport (CVT) method in a sealed quartz tube as can be seen from the schematic diagram in Figure 1a. The scanning electron microscopy (SEM) image of the as prepared hexagonal FePS<sub>3</sub> sheet, with a size about 200 μm, and the corresponding energy dispersive X-ray spectroscopy (EDS) elemental mapping images are clearly shown in Figure 1b. More crystal structures of the bulk FePS<sub>3</sub> are displayed in Figures S1 and S2 in the Supporting Information. To obtain the desired FePS<sub>3</sub> Qs, a two-step exfoliation method was implemented. First, the prepared bulk FePS<sub>3</sub> was intercalated by reacting with hydrazine (N<sub>2</sub>H<sub>4</sub>) in hydrothermal condition (Figure 1c). Second, the intercalated FePS<sub>3</sub> crystals were exfoliated by sonication at a high power of 100 W for 4 h to form the Qs, as shown in Figure 1d. It can be seen that the Qs are evenly distributed on the substrate. The statistical distribution of the diameter (inset) illustrates that the isolated Qs tend to be 4–8 nm in size. This may provide better homogeneity for further characterization and testing. More transmission electron microscopy (TEM) images of the Qs are depicted in Figure S3 of the Supporting Information. It is obvious that the FePS<sub>3</sub> Qs, with the size below 10 nm, are well dispersed on the ultrathin carbon film with a homogeneous thickness (Figure S3b,c, Supporting Information). The mechanism of the exfoliation processes can reasonably be explained by a redox rearrangement model.<sup>[20]</sup> At the first glance, part of the N<sub>2</sub>H<sub>4</sub> were oxidized to N<sub>2</sub>H<sub>5</sub><sup>+</sup>

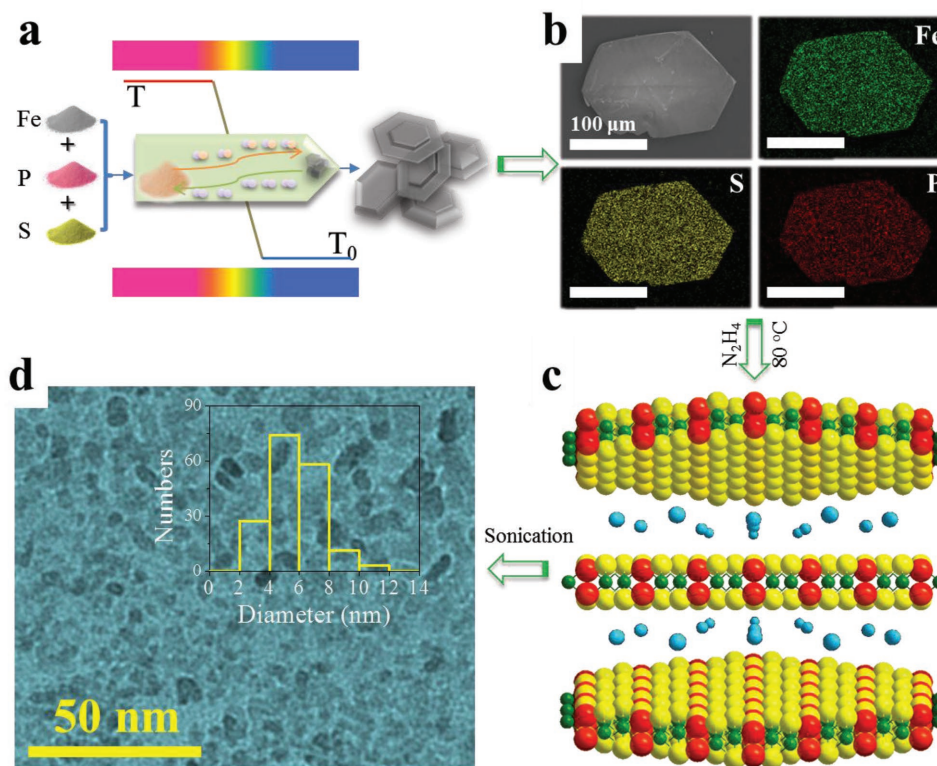


**Figure 1.** Preparation of the FePS<sub>3</sub> bulk and Qs. a) The schematic of chemical vapor transport (CVT) method. b) SEM and the corresponding EDS elemental mapping images of a bulk FePS<sub>3</sub> as prepared. c) The decomposition product of pre-exfoliated bulk FePS<sub>3</sub> (Fe: green, P: red, S: yellow). d) The TEM image of the FePS<sub>3</sub> Qs. A diameter statistic of the size distribution of FePS<sub>3</sub> Qs is given in the inset.

during intercalation. Up on heating, the intercalated  $N_2H_5^+$  was decomposed to different gaseous species such as  $N_2$ ,  $NH_3$ , and  $H_2$  owing to its poor thermal stability. This brought the formation of expanded crystals in  $FePS_3$ , which after were treated at high power sonication. The ultrasonic waves in solvent would generate cavitation bubbles and then collapse into high-energy jets, breaking up the expanded crystals and producing QSSs. In addition, modeling has shown that if the surface energy of the solvent is similar to that of the layered material, the energy difference between the exfoliated and reaggregated states will be very small, removing the driving force for reaggregation.<sup>[21–23]</sup> For example, graphene, h-BN, transition metal dichalcogenides materials, and some transition metal oxide materials have been exfoliated by using suitable solvents such as *N*-methyl-pyrrolidone.<sup>[24]</sup> In our system,  $FePS_3$  material was estimated to have a surface energy of  $\approx 100 \text{ mJ m}^{-2}$ .<sup>[9,25]</sup> On the other hand, the solvent surface energy is related to the surface tension by<sup>[23]</sup>

$$E_{\text{sur}}^{\text{sol}} = \gamma + TS_{\text{sur}}^{\text{sol}} \quad (1)$$

where  $\gamma$  is the solvent surface tension ( $\text{mN m}^{-1}$ ),  $E_{\text{sur}}^{\text{sol}}$  is the solvent surface energy ( $\text{mJ m}^{-2}$ ),  $T$  is the temperature ( $\approx 300 \text{ K}$ ), and  $S_{\text{sur}}^{\text{sol}}$  is the solvent surface entropy ( $\approx 0.1 \text{ mJ m}^{-2} \text{ K}^{-1}$ ). Given the surface tension of water ( $\gamma = 72 \text{ mN m}^{-1}$  at  $300 \text{ K}$ ) and hydrazine hydrate ( $\gamma = 74 \text{ mN m}^{-1}$  at  $300 \text{ K}$ ), their surface energy can be calculated as  $102$  and  $104 \text{ mJ m}^{-2}$ , respectively, which are very close to that of  $FePS_3$ . This result means that

water and hydrazine hydrate are suitable solvents to realize the successful exfoliation into monolayer  $FePS_3$  QSSs.

In order to have a detailed examination of the samples, we characterized the obtained materials by high-resolution transmission electron microscopy (HRTEM). The HRTEM image of the bulk  $FePS_3$  was shown Figure 2a. The space of  $0.321 \text{ nm}$  can be indexed to the (002) plane of  $FePS_3$ . A clear observation is apparent from Figure 2b from which a  $\approx 7 \text{ nm}$  diameter of quantum sheet (QS) can be seen. Furthermore, the lattice stripes with space of  $0.186 \text{ nm}$  belonging to the (310) plane of  $FePS_3$  are observed, solidly corroborating the formation of the desired material. More details about the crystal structure of the bulk and QSSs are displayed in Figures S3–S5 in the Supporting Information. For visualization through atomic force microscopy (AFM), the  $FePS_3$  QSSs were drop-casted onto sapphire, by a  $20 \mu\text{L}$  pipette. The thickness profile of the QSSs reveals that most of the QSSs are monolayers (Figure S6, Supporting Information).

To further confirm the crystallographic assertion, the X-ray diffraction (XRD) patterns of the  $FePS_3$  bulk and QSSs were obtained and displayed in Figure 2c. Besides the peaks belonging to fluorine-doped tin oxide (FTO) substrate (The International Centre for Diffraction Data (ICDD), PDF#46-1088), a perfect alignment with the standard card (ICDD, PDF#30-0663) for all the peaks of bulk  $FePS_3$  suggests the high phase purity of our synthesized material. The sharp peaks at  $13.8^\circ$  and  $27.8^\circ$  can be indexed to (001) and (002) planes of the  $FePS_3$  crystals, respectively. Comparing the QSSs with the bulk, it is obvious that the peak at  $13.8^\circ$  is disappeared

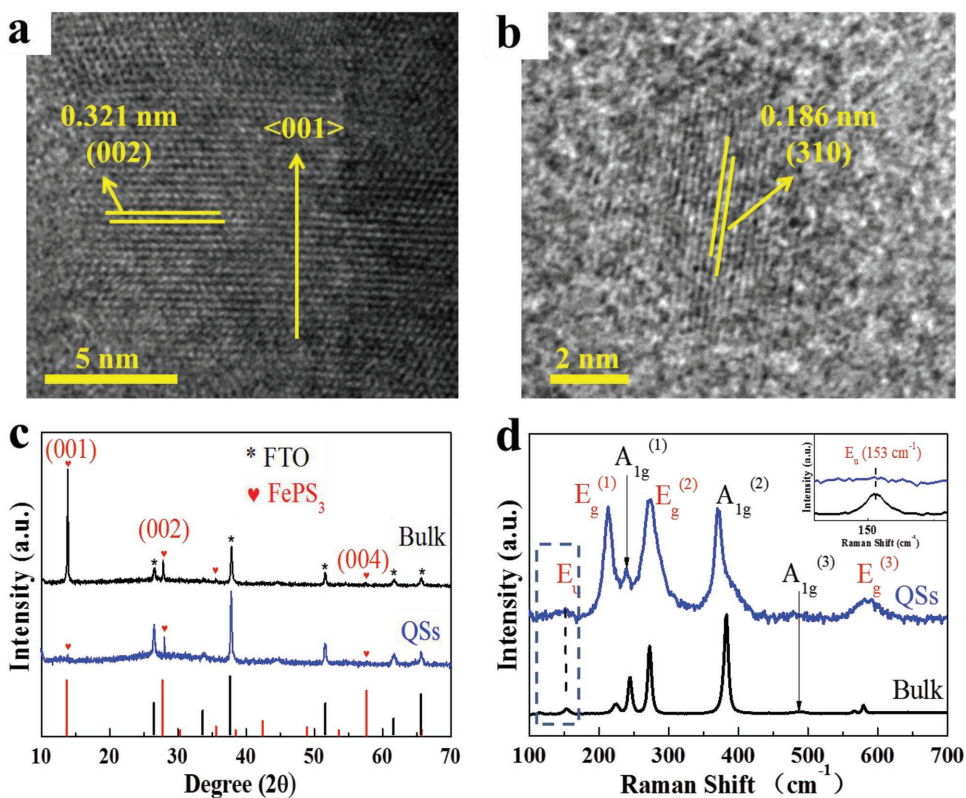


**Figure 2.** Characterization of the  $FePS_3$  bulk and QSSs. HRTEM of: a) the  $FePS_3$  bulk and b) QSSs. c) XRD and d) Raman spectra of the bulk and QSSs samples.



for the case of QSSs. This can be attributed to the diminishing of (001) plane as the bulk FePS<sub>3</sub> crystals is transformed into monolayer. We also characterized the surface chemical states by X-ray photoelectron spectroscopy (XPS), shown in Figure S7 in the Supporting Information. Accordingly, the high-resolution XPS spectra of Fe 2p region indicate that the oxidation state of Fe in FePS<sub>3</sub> is +2. A critical comparison of XPS spectra (bulk vs QSSs) reveals that there is no obvious change on the surface chemical states, further corroborating the safety and stability of our exfoliation method.

The analysis of Raman spectra gives more insight understanding of the distinction between the bulk and monolayer QSSs, displayed in Figure 2d. According to the report by Scagliotti et al.,<sup>[26]</sup> the Raman modes of FePS<sub>3</sub> originate from two parts of the crystal structure (the vibrations of metal atom and the P<sub>2</sub>S<sub>6</sub> unit, which belongs to the D<sub>3d</sub> symmetry group). Three A<sub>1g</sub>-type modes (polarized, A<sub>1g</sub><sup>(1-3)</sup>) and three E<sub>g</sub>-type modes (depolarized, E<sub>g</sub><sup>(1-3)</sup>) from the vibrations of the P<sub>2</sub>S<sub>6</sub> unit could be resolved in the spectra (Figure S8, Supporting Information). As shown in Figure 2d, the peaks at 214 cm<sup>-1</sup> (E<sub>g</sub><sup>(1)</sup>), 240 cm<sup>-1</sup> (A<sub>1g</sub><sup>(1)</sup>), 274 cm<sup>-1</sup> (E<sub>g</sub><sup>(2)</sup>), 372 cm<sup>-1</sup> (A<sub>1g</sub><sup>(2)</sup>), and 586 cm<sup>-1</sup> (E<sub>g</sub><sup>(3)</sup>) can be assigned to the FePS<sub>3</sub> QSSs, and those at 153 cm<sup>-1</sup> (E<sub>u</sub>), 223 cm<sup>-1</sup> (E<sub>g</sub><sup>(1)</sup>), 245 cm<sup>-1</sup> (A<sub>1g</sub><sup>(1)</sup>), 272 cm<sup>-1</sup> (E<sub>g</sub><sup>(2)</sup>), and 382 cm<sup>-1</sup> (A<sub>1g</sub><sup>(2)</sup>), 486 cm<sup>-1</sup> (A<sub>1g</sub><sup>(3)</sup>), and ≈580 cm<sup>-1</sup> (E<sub>g</sub><sup>(3)</sup>) can be associated to the bulk FePS<sub>3</sub>.<sup>[26-28]</sup> The A<sub>1g</sub> modes represent the stretching vibration of the P–P band, which indicate the out-of plane vibrations of the P<sub>2</sub>S<sub>6</sub> unit (Figure S8, Supporting Information). The A<sub>1g</sub><sup>(1)</sup> is due to the opposite movement of the S<sub>3</sub>P–PS<sub>3</sub> unit, which has been found very sensitive to alkali-ion intercalation and to the c-axis expansion. Moreover, the A<sub>1g</sub><sup>(2)</sup> and A<sub>1g</sub><sup>(3)</sup> modes represent the symmetric stretching vibration of the P–S bonds and the relative movement of the S<sub>3</sub>P–PS<sub>3</sub> unit, respectively. Moreover, the E<sub>g</sub> modes are meant for the tangential vibration of the P–P bond, which indicate the in-plane vibrations of the P<sub>2</sub>S<sub>6</sub> unit (Figure S8, Supporting Information). The E<sub>g</sub><sup>(1)</sup> and E<sub>g</sub><sup>(2)</sup> are active in two orthogonal scattering geometries where as the E<sub>g</sub><sup>(3)</sup> is sensitive to the lattice distortions.<sup>[26]</sup> The peak at about 153 cm<sup>-1</sup> is the Raman counterpart of the strongly infrared active E<sub>u</sub>-type mode of the P<sub>2</sub>S<sub>6</sub> unit observed in all members of the MPS<sub>3</sub> compound absorption spectra.

When the unit cell is doubled along the c axis, the out-of-plane vibration of two P<sub>2</sub>X<sub>6</sub> units in adjacent layers becomes Raman active.<sup>[26,29]</sup> From the inset of Figure 2d, the absence of E<sub>u</sub> peak in QSSs sample suggests the achievement of monolayer FePS<sub>3</sub> QSSs.

To explore the optical properties of the FePS<sub>3</sub> bulk and QSSs, UV/vis/NIR diffuse-reflection spectra (DRS) and ultraviolet photoelectron spectroscopy (UPS) were used and the results are shown in Figure 3. According to the Kubelka–Munk theory, the absorption coefficient ( $\alpha$ ) could be obtained by the Kubelka–Munk function ( $F(R)$ ) from the diffuse reflectance measurement.<sup>[30]</sup> Also, the bandgap energy of the material is estimated by the intercept of the tangent to the X-axis ( $h\nu$ ) in the Tauc plot<sup>[31]</sup> (inset of Figure 3a). The FePS<sub>3</sub> is known to be an indirect bandgap semiconductor so that the  $(\alpha h\nu)^{1/2}$  instead of  $(\alpha h\nu)^2$  is set as the Y-axis for contracting the Tauc plot.<sup>[32]</sup> Accordingly, the bandgap values of FePS<sub>3</sub> bulk and QSSs are found to be 1.60 and 2.18 eV, respectively (Figure 3a, inset). The UPS was used to determine the valence band energy level (E<sub>v</sub>) of the bulk and QSSs, as shown in Figure 3b. Through subtracting the width of He I UPS spectra from the excitation energy (21.22 eV), the E<sub>v</sub> values were calculated to be –5.40 eV for the bulk and –5.57 eV for the QSSs (vs E<sub>Vacuum</sub>), respectively. Then the conduction band energy (E<sub>c</sub>) of the material can be calculated by E<sub>v</sub>–E<sub>g</sub> (–3.80 eV for bulk and –3.39 eV for QSSs). As a matter of fact, QSSs exhibit a wider bandgap (2.18 eV), compared to the bulk (1.60 eV). No matter how the FePS<sub>3</sub> QSSs display a more negative overpotential than H<sup>+</sup>/H<sub>2</sub> (–0.20 V for bulk and –0.61 V for QSSs, vs NHE, PH = 7), the feature of QSSs enables the accumulation of abundant hot electrons at E<sub>c</sub> for catalyzing the hydrogen evolution reaction (Figure S9, Supporting Information).

Having seen the well-exfoliated QSSs of FePS<sub>3</sub> and the appropriately positioned E<sub>c</sub> level for sunlight driven catalysis of H<sub>2</sub> gas production, we conducted photocatalytic hydrogen evolution experiments in aqueous solution containing 10 vol% triethanolamine (TEOA) as the hole scavenger. The performance of bulk FePS<sub>3</sub> was also measured under exactly the same condition for the sake of comparison. As can be seen in Figure 4a, FePS<sub>3</sub> QSSs show a high efficiency of 290 μmol h<sup>-1</sup> g<sup>-1</sup> compared with the significantly lower value of 94 μmol h<sup>-1</sup> g<sup>-1</sup> for

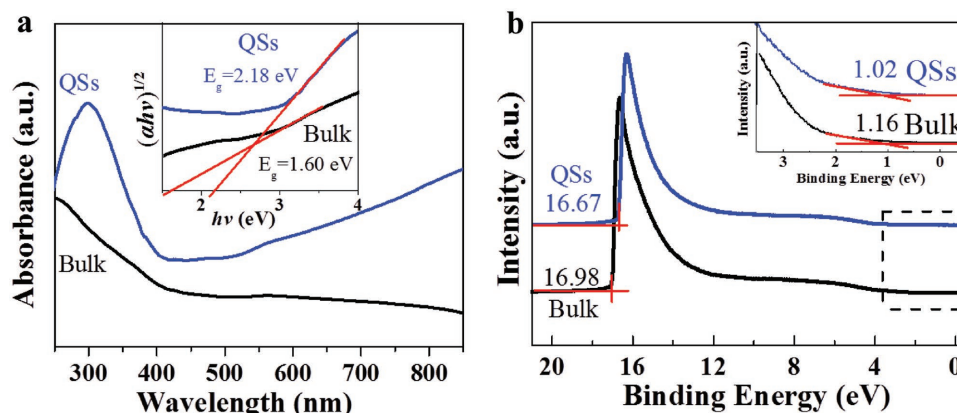


**Figure 3.** Optical properties of the FePS<sub>3</sub> bulk and QSSs. a) UV/vis/NIR diffusive reflectance absorption spectra and estimated bandgap potential (inset) of synthesized FePS<sub>3</sub> bulk (1.60 eV) and QSSs (2.18 eV). b) UPS spectra of the bulk and QSSs, in which the dashed red lines mark the baseline and the tangents of the curve.

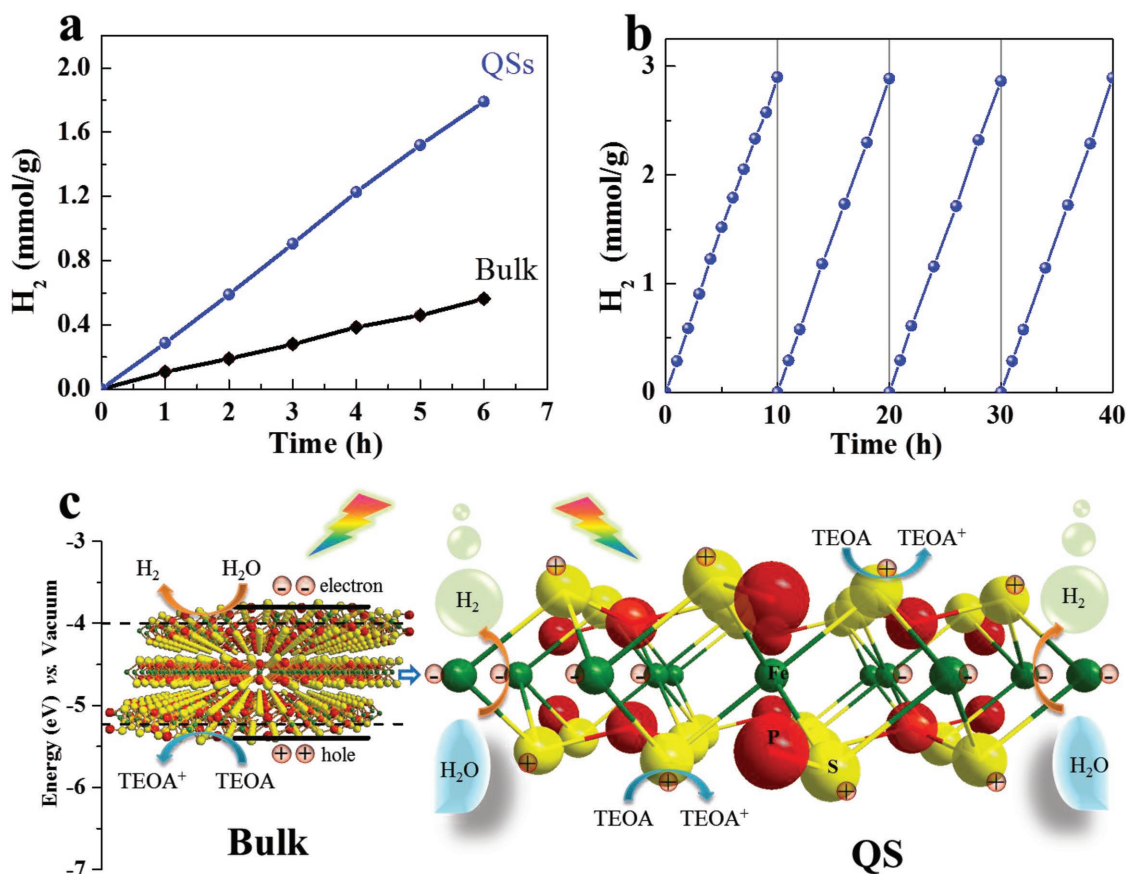


**Figure 4.** photocatalytic performance of the FePS<sub>3</sub> bulk and QDs. a) Plots of hydrogen production through direct photocatalytic water splitting of the FePS<sub>3</sub> bulk and QDs, in 100 mL deionized water with 10% TEOA as sacrificial agent. b) Cycling measurements of hydrogen gas generation of the FePS<sub>3</sub> QDs. c) Schematics of photocatalytic reaction processes for the FePS<sub>3</sub> bulk and QDs.

bulk FePS<sub>3</sub>. Furthermore, the stability of QDs for hydrogen production was evaluated and the result is depicted in Figure 4b. The sample exhibits a feasible ability in the cycling measurements of H<sub>2</sub> generation under light illumination for a continuous 40 h test. This enhancement can be attributed to the great amount of exposed boundaries providing more active sites and efficient separation of photogenerated electrons in QDs. From such all dimensional quantum confinement, it can be inferred that there are significant differences from the bulk in photocatalytic reaction, as shown in Figure 4c. Under the light illumination, the photogenerated electron and hole are located in the conduction band and valence band separately. The photogenerated electrons are consumed to produce H<sub>2</sub> molecules while the photogenerated holes are used to oxidize the sacrificial agent (TEOA). Exfoliating the bulk into monolayered FePS<sub>3</sub> QDs highly contributes to the increase in surface area/active sites, which is beneficial for the enhancement of photocatalytic activity.

In summary, we have developed a facile way to obtain monolayer FePS<sub>3</sub> QDs from the bulk FePS<sub>3</sub>, which was first prepared by CVT method. The QDs demonstrate a lateral size below 10 nm. The exfoliation method brought no change on the chemical composition and state of the elements in FePS<sub>3</sub>. Given the 3D confinement, there resulted an associated change in the electronic band structure of the obtained QDs as

compared to the bulk. A three times performance enhancement (290 μmol h<sup>-1</sup> g<sup>-1</sup> for the QDs and 94 μmol h<sup>-1</sup> g<sup>-1</sup> for bulk) is observed for QDs in photocatalytic hydrogen evolution reaction that can be attributed to the monolayer effects. We believe that these facilely synthesized monolayer QDs can also find a very promising performance in other applications as well.

## Experimental Section

**Preparation of FePS<sub>3</sub> Powders:** A stoichiometric amount of high-purity elements (Fe: 99.99%, P: 99.999%, S: 99.99%,) and iodine (30 mg) as a transport agent were sealed into a quartz tube under vacuum and heated at 700 °C for two weeks. After cooled down to room temperature, a product of black powder with metallic luster was obtained.

**Preparation of FePS<sub>3</sub> QDs:** The as-synthesized bulk FePS<sub>3</sub> (30 mg) with 20 mL of hydrazine hydrate (80%) was sealed in an autoclave and heated at 80 °C for 4 h. The mixture was then sonicated in a high-power sonic bath (100 W) for 4 h to form a homogeneous suspension. Eventually, the desired FePS<sub>3</sub> QDs were obtained by a centrifugal separation at 8000 rpm for 15 min to remove unexfoliated material. For the further measurements, the QDs were spin-coated on the FTO and dried at 60 °C for 24 h.

**Characterization of Materials:** SEM and the corresponding EDS mapping images were obtained from a Hitachi S4800 field-emission scanning electron microanalyzer with EDS. TEM and HRTEM images were obtained via employing a Tecnai G2 F20 with beam energy of 200 keV. The thickness was analyzed by AFM (MFP-3D Infinity). XRD

patterns were collected from a D/MAX-TTRIII(CBO) system using a Cu-K $\alpha$  radiation ( $\lambda = 1.5418 \text{ \AA}$ ). Raman spectroscopy was measured at room temperature on an inVia Renishaw system at the excitation line of 532 nm. The Raman peak of Si at  $520 \text{ cm}^{-1}$  was used as a reference to calibrate the spectrometer. XPS was performed on the Thermo Scientific ESCALab 250Xi using 200 W monochromatic Al K $\alpha$  radiation. The  $500 \text{ }\mu\text{m}$  X-ray spot was used for SAXPS analysis. The base pressure in the analysis chamber was about  $3 \times 10^{-9}$  mbar. Typically, the hydrocarbon C1s line at 284.8 eV from adventitious carbon is used for energy referencing. UV/vis/NIR DRS were recorded on a Lambda 750 spectrophotometer equipped with an integrating sphere. The valence band energy of the samples was analyzed on Thermo Scientific ESCALab 250Xi using UPS. The gas discharge lamp was used for UPS, with helium gas admitted and the HeI (21.22 eV) emission line employed. The helium pressure in the analysis chamber during analysis was about  $2 \times 10^{-8}$  mbar. The data were acquired with  $-10 \text{ V}$  bias.

**Measurement of Photocatalytic H<sub>2</sub> Evolution:** Photocatalytic water splitting experiments were conducted in a 500 mL cylinder quartz reactor at ambient temperature. A 300 W xenon lamp used as a light source. In a typical H<sub>2</sub> evolution experiment, the prepared photocatalyst (on FTO, about  $0.6 \text{ mg cm}^{-2}$ ) was placed at the bottom of reactor containing 100 mL of aqueous solution with 10% TEOA. Before irradiation, the system was vacuumed for about 30 min to remove the air inside and to ensure that the system was under the anaerobic condition. A certain amount of gas was intermittently sampled and analyzed by gas chromatography (GC7900, Shimadzu, Japan, TCD, nitrogen as a carrier gas and 5  $\text{\AA}$  molecular sieve column) by using Ar as a carrier gas. A baseline was recorded for each test before exposure to xenon lamp.

## Supporting Information

Supporting Information is available from the Wiley Online Library or from the author.

## Acknowledgements

This work was supported by the Ministry of Science and Technology of China (No. 2016YFA0200700), the National Natural Science Foundation of China (Nos. 21703047, 21373065, 61474033, 61574050, and 11674072), Strategic Priority Research Program of the Chinese Academy of Sciences (Grant No. XDA09040201), and CAS Key Laboratory of Nanosystem and Hierarchical Fabrication. The authors also gratefully acknowledge the support of Youth Innovation Promotion Association CAS.

## Conflict of Interest

The authors declare no conflict of interest.

## Keywords

chemical exfoliation, FePS<sub>3</sub>, monolayer quantum sheets, water splitting

Received: December 20, 2017

Revised: March 15, 2018

Published online:

- [1] K. S. Novoselov, A. K. Geim, S. V. Morozov, D. Jiang, Y. Zhang, S. V. Dubonos, I. V. Grigorieva, A. A. Firsov, *Science* **2004**, 306, 666.
- [2] B. Radisavljevic, A. Radenovic, J. Brivio, i. V. Giacometti, A. Kis, *Nat. Nanotechnol.* **2011**, 6, 147.
- [3] X. Wang, K. Maeda, A. Thomas, K. Takane, G. Xin, J. M. Carlsson, K. Domen, M. Antonietti, *Nat. Mater.* **2009**, 8, 76.
- [4] K. F. Mak, C. Lee, J. Hone, J. Shan, T. F. Heinz, *Phys. Rev. Lett.* **2010**, 105, 136805.
- [5] B. L. Chittari, Y. Park, D. Lee, M. Han, A. H. MacDonald, E. Hwang, J. Jung, *Phys. Rev. B* **2016**, 94, 184428.
- [6] A. Wildes, V. Simonet, E. Ressouche, G. J. McIntyre, M. Avdeev, E. Suard, S. Kimber, D. Lançon, G. Pepe, B. Moubaraki, *Phys. Rev. B* **2015**, 92, 224408.
- [7] J.-U. Lee, S. Lee, J. H. Ryoo, S. Kang, T. Y. Kim, P. Kim, C.-H. Park, J. G. Park, H. Cheong, *Nano Lett.* **2016**, 16, 7433.
- [8] M. A. Susner, M. Chyasnavichyus, M. A. McGuire, P. Ganesh, P. Maksymovych, *Adv. Mater.* **2017**, 29, 1602852.
- [9] X. Zhang, X. Zhao, D. Wu, Y. Jing, Z. Zhou, *Adv. Sci.* **2016**, 3, 1600062.
- [10] Y. Cai, G. Zhang, Y. W. Zhang, *J. Am. Chem. Soc.* **2014**, 136, 6269.
- [11] F. Wang, T. A. Shifa, P. He, Z. Cheng, J. Chu, Y. Liu, Z. Wang, F. Wang, Y. Wen, L. Liang, *Nano Energy* **2017**, 40, 673.
- [12] T. A. Shifa, F. M. Wang, Z. Z. Cheng, P. He, Y. Liu, C. Jiang, Z. Wang, J. He, *Adv. Funct. Mater.* **2018**, 28, 1800548.
- [13] X. Y. Liu, H. Chen, R. Wang, Y. Shang, Q. Zhang, W. Li, G. Zhang, J. Su, C. T. Dinh, F. de Arquer, *Adv. Mater.* **2017**, 29, 1605646.
- [14] S. Zhou, N. Liu, J. Zhao, *Comput. Mater. Sci.* **2017**, 130, 56.
- [15] M. Zamkov, *Nat. Energy* **2017**, 2, 17072.
- [16] J. B. Sambur, T. Novet, B. Parkinson, *Science* **2010**, 330, 63.
- [17] R. Zacharia, H. Ulbricht, T. Hertel, *Phys. Rev. B* **2004**, 69, 155406.
- [18] X. Li, X. Wu, J. Yang, *J. Am. Chem. Soc.* **2014**, 136, 11065.
- [19] D. Mukherjee, P. M. Austeria, S. Sampath, *ACS Energy Lett.* **2016**, 1, 367.
- [20] J. Zheng, H. Zhang, S. Dong, Y. Liu, C. T. Nai, H. S. Shin, H. Y. Jeong, B. Liu, K. P. Loh, *Nat. Commun.* **2014**, 5, 2995.
- [21] V. Nicolosi, M. Chhowalla, M. G. Kanatzidis, M. S. Strano, J. N. Coleman, *Science* **2013**, 340, 1226419.
- [22] J. N. Coleman, *Acc. Chem. Res.* **2012**, 46, 14.
- [23] Y. Hernandez, V. Nicolosi, M. Lotya, F. M. Blighe, Z. Sun, S. De, I. McGovern, B. Holland, M. Byrne, Y. K. Gun'Ko, *Nat. Nanotechnol.* **2008**, 3, 563.
- [24] J. N. Coleman, M. Lotya, A. O'Neill, S. D. Bergin, P. J. King, U. Khan, K. Young, A. Gaucher, S. De, R. J. Smith, *Science* **2011**, 331, 568.
- [25] T. Björkman, A. Gulans, A. V. Krasheninnikov, R. M. Nieminen, *Phys. Rev. Lett.* **2012**, 108, 235502.
- [26] M. Scagliotti, M. Jouanne, M. Balkanski, G. Ouvrard, G. Benedek, *Phys. Rev. B* **1987**, 35, 7097.
- [27] K. Z. Du, X. Z. Wang, Y. Liu, P. Hu, M. I. B. Utama, C. K. Gan, Q. Xiong, C. Kloc, *ACS Nano* **2015**, 10, 1738.
- [28] X. Wang, K. Du, Y. F. Liu, P. Hu, J. Zhang, Q. Zhang, M. H. S. Owen, X. Lu, C. K. Gan, P. Sengupta, *2D Mater.* **2016**, 3, 031009.
- [29] Y. Mathey, R. Clement, C. Sourisseau, G. Lucazeau, *Inorg. Chem.* **1980**, 19, 2773.
- [30] Y. C. Zhang, Z. N. Du, K. W. Li, M. Zhang, D. D. Dionysiou, *ACS Appl. Mater. Interfaces* **2011**, 3, 1528.
- [31] P. Chen, Y. Su, H. Liu, Y. Wang, *ACS Appl. Mater. Interfaces* **2013**, 5, 12073.
- [32] Z. Cheng, F. Wang, T. A. Shifa, C. Jiang, Q. Liu, J. He, *Small* **2017**, 13, 1702163.